

## Video Article

# Ultrasound Imaging of the Thoracic and Abdominal Aorta in Mice to Determine Aneurysm Dimensions

Hisashi Sawada<sup>1</sup>, Jeff Z. Chen<sup>2</sup>, Bradley C. Wright<sup>1</sup>, Jessica J. Moorlegghen<sup>1</sup>, Hong S. Lu<sup>1,2</sup>, Alan Daugherty<sup>1,2</sup>

<sup>1</sup>Saha Cardiovascular Research Center, University of Kentucky

<sup>2</sup>Department of Physiology, University of Kentucky

Correspondence to: Alan Daugherty at [alan.daugherty@uky.edu](mailto:alan.daugherty@uky.edu)

URL: <https://www.jove.com/video/59013>

DOI: [doi:10.3791/59013](https://doi.org/10.3791/59013)

Keywords: Medicine, Issue 145, Ultrasound imaging, aortic dimensions, aorta, aortic sinus, ascending aorta, abdominal aorta, aortic aneurysm

Date Published: 3/8/2019

Citation: Sawada, H., Chen, J.Z., Wright, B.C., Moorlegghen, J.J., Lu, H.S., Daugherty, A. Ultrasound Imaging of the Thoracic and Abdominal Aorta in Mice to Determine Aneurysm Dimensions. *J. Vis. Exp.* (145), e59013, doi:10.3791/59013 (2019).

## Abstract

Contemporary high-resolution ultrasound instruments have sufficient resolution to facilitate the measurement of mouse aortas. These instruments have been widely used to measure aortic dimensions in mouse models of aortic aneurysms. Aortic aneurysms are defined as permanent dilations of the aorta, which occur most frequently in the ascending and abdominal regions. Sequential measurements of aortic dimensions by ultrasound are the principal approach for assessing the development and progression of aortic aneurysms in vivo. Although many reported studies used ultrasound imaging to measure aortic diameters as a primary endpoint, there are confounding factors, such as probe position and cardiac cycle, that may impact the accuracy of data acquisition, analysis, and interpretation. The purpose of this protocol is to provide a practical guide on the use of ultrasound to measure the aortic diameter in a reliable and reproducible manner. This protocol introduces the preparation of mice and instruments, the acquisition of appropriate ultrasound images, and data analysis.

## Video Link

The video component of this article can be found at <https://www.jove.com/video/59013/>

## Introduction

Aortic aneurysms are common vascular diseases characterized by a permanent luminal dilation of the thoracic and/or abdominal aorta<sup>1,2,3,4</sup>. No pharmacological therapies have been established to prevent the dilation and rupture of aortic aneurysms, which emphasizes the need for insights into pathogenic mechanisms. To elucidate the mechanisms of aortic aneurysms, mouse models produced by genetic or chemical manipulations have been widely used<sup>4,5,6,7,8,9,10,11,12</sup>. The accurate quantification of the aortic diameter in mice is the basis of aortic aneurysm research.

The development of high-frequency ultrasound has increased the spatial and temporal resolution of images to detect small differences in aortic dimensions<sup>13,14,15</sup>. This has enabled the sequential measurement of aortic diameters in mice, and thus, it has become the preferred method for measuring aortic diameters in murine studies of aortic aneurysms. Although ultrasound imaging is a simple technique, knowledge of aortic anatomy and physiology is required to acquire appropriate images for accurate measurements, data analysis, and interpretation. The aorta is a pulsating cylindrical organ with variable curvatures in the proximal thoracic region<sup>16</sup>. This contributes to the potential for an inaccurate determination of aortic dimensions in the commonly acquired two-dimensional (2D) images. The accuracy of aortic measurements could be compromised further by aortic tortuosity in aneurysmal state<sup>17</sup>. To obtain reliable and reproducible measurements of aortic dilations, this protocol provides a practical guide for the use of a high-resolution ultrasound system to measure proximal thoracic and abdominal aortic diameters in mice.

## Protocol

Ultrasound imaging in mice is performed with approval of the University of Kentucky Institutional Animal Care and Use Committee (IACUC protocol number: 2018-2967). During the imaging, the mice are anesthetized using isoflurane 1%–3% vol/vol and placed on a heating platform to reduce procedural stress and prevent hypothermia. Eye lubricant is applied to prevent corneal damage due to the loss of the blink reflex during anesthesia.

## 1. Equipment Setup

1. Turn on the ultrasound machine, heating platform, and gel warmer (**Figure 1**).
2. Open the ultrasound program. Enter the study information, such as the study name and mouse information.
3. Check the isoflurane vaporizer and O<sub>2</sub> tank. If the content is low, fill the isoflurane vaporizer and/or exchange it for a new O<sub>2</sub> tank.

4. Connect the anesthetic scavenging filters to the induction chamber and the nose cone.
5. Open the branch for the induction chamber.
6. Turn on the O<sub>2</sub> tank.
7. Turn the O<sub>2</sub> and isoflurane knobs on the anesthesia vaporizer to 1 L/min and 0% vol/vol, respectively, to fill the chamber with O<sub>2</sub>.

## 2. Preparation of the Mouse

1. Place the mouse in the O<sub>2</sub>-filled induction chamber to minimize unwanted cardiovascular changes due to anesthesia.
2. Turn on the isoflurane vaporizer (1.5%–2.5 % vol/vol).
3. Confirm the absence of the hind limb withdrawal reflex.
4. Remove the mouse from the chamber and place one drop of sterile ophthalmic lubricant in each eye.
5. Redirect the anesthesia to the nose cone and close the flow to the induction chamber.
6. Lay the mouse dorsally on the heating platform with its nose in the anesthesia nose cone.
7. Apply depilatory cream to the chest or abdomen, using a cotton swab. Minimize the amount of depilatory cream use to avoid irritation.
8. Wait for 1 min, and then, gently wipe off all cream and hair.
9. Irrigate the area with warm water and wipe it dry to completely remove the cream.
10. Dot gel on each of the four copper leads on the platform.
11. Tape each paw pad down (palms down) to the leads for electrocardiogram (ECG) readings. This will provide the ECG and respiratory physiology of the mouse while anesthetized.
12. Verify that the heart rate is between 450–550 beats/min. Since anesthesia affects cardiac function, which can alter the aortic diameter, adjust the delivery rate of anesthesia so that the heart rate is in an appropriate range.
13. Apply prewarmed ultrasonic gel to the prepared site.
14. Attach the probe to the holder.
15. Rotate the platform for optimal scanning and lower the probe until it is in contact with the ultrasonic gel.

## 3. Imaging of the Thoracic Aorta

1. Tilt down the platform to the left side of the mouse.
2. Put the probe on the right edge of the mouse's sternum (**Figure 2A**). Orient the reference marker on the probe caudally.  
**NOTE:** The reference marker on the probe indicates the probe direction and is consistent with the marker on the monitor of the ultrasound system (**Figure 2A-D**). The shape of the marker varies in each ultrasound system.
3. Use color Doppler on the thoracic aorta to confirm blood flow.
4. Adjust the stage and probe angle to show the aorta clearly (**Figure 3A,B**).  
**NOTE:** The aortic valve and innominate and pulmonary arteries can be used for anatomical landmarks for the right parasternal long axis view. Therefore, aortic images from this view can include the aortic valve and innominate and pulmonary arteries in one frame (**Figure 3A**). If it is difficult to capture the entire ascending aorta in one scan, due to aortic pathologies such as aortic dilation and tortuosity, the images should be captured separately. Since separated images have the potential to cause an underestimation of the aortic measurements, fine positioning of the stage and probe is required. The right parasternal long axis view is optimal for imaging the entire ascending aorta (**Figure 3C**). However, it is often difficult to capture the aortic sinus in this view, especially in aneurysmal aortas. The left parasternal long axis view enables a capture from the aortic root to the proximal ascending aorta as an alternative approach, although this view cannot capture the aortic arch in one frame (**Figure 3C**). For the left parasternal long axis view, put the probe on the left edge of the sternum (**Figure 2B**). The stage is flat or slightly tilted to the mouse's right. Carry out the other steps of the procedure in the same manner as the right parasternal long axis view. Advantages and disadvantages of these probe positions are described in **Table 2**. Aortic images must be captured consistently in either right or left parasternal long axis view.
5. Crop the ultrasound image to increase the frame rate, using the knobs for image depth and width.
6. Change the focal depth on the dorsal side of the ascending aorta, using the knob for focal depth.
7. Verify the ultrasound parameters. The ultrasound settings for this protocol are described in **Table 1**.
8. Move the probe gently, using the X- and Y-axis stage knob, to capture the longitudinal aortic image with the largest possible diameter.
9. Store one cine loop.

## 4. Imaging of the Abdominal Aorta

1. Place the probe transversely, just below the sternum and xiphoid process (**Figure 2C**). The reference marker on the probe should face the mouse's right side. The abdominal aorta should be located next to the inferior vena cava and/or portal vein (**Figure 3D**).
2. Visualize the abdominal aorta with color Doppler to confirm pulsatile flow.  
**NOTE:** If the Doppler angle is perpendicular to the blood flow, a color Doppler signal will not appear in the aorta. In addition to color Doppler imaging, the abdominal aorta can be distinguished from the vena cava and portal vein by slightly pressing down the probe. The vena cava and portal vein are compressible, while the aorta maintains its patency.
3. Crop the ultrasound image to increase the frame rate.
4. Change the focal depth to the posterior wall of the abdominal aorta.
5. Move the probe caudally to visualize the branch points of the celiac and superior mesenteric arteries.
6. Locate the right renal artery and use it as a landmark.  
**NOTE:** Since abdominal aortic aneurysms may lead to aortic tortuosity, adjust the probe angle to image the abdominal aorta perpendicularly. For an internal control, one image of the right renal branch point should be captured.
7. Capture a cine loop of the region of interest which shows the maximum dilation in the abdominal aorta (**Figure 3D,E**).  
**NOTE:** The localization of aortic aneurysms varies in each animal model. Aortic dilation in angiotensin II-induced mice occurs predominantly in the suprarenal aorta, while CaCl<sub>2</sub> or elastase induces aortic aneurysm in the infrarenal aorta in mice.

## 5. Postscanning Mouse Care and Cleanup

1. Wipe off the ultrasonic gel, irrigate the chest or abdomen with warm water, and gently wipe the mouse dry.
2. Return the mouse to its cage, which is placed on a heating pad.
3. Turn off the isoflurane vaporizer and O<sub>2</sub> tank. Refill the vaporizer if the isoflurane level is low.
4. Clean the ultrasound machine, probe, and platform with a soft cloth and isopropyl alcohol or glutaraldehyde wipes.
5. Download all files collected during the scan.
6. Turn off the ultrasound machine.
7. Return the mice to animal housing rooms after they have recovered from the anesthesia.

## 6. Analysis

### 1. Analysis of thoracic aortic images

1. Launch the analysis software and open the ultrasound data. An example image of analysis software (Vevo LAB 3.0.0) is shown in **Supplemental Figure 1**.
2. Select one aortic ultrasound image for measurements from the cine loop (**Figure 4A,C,E,G** and **Supplemental Figure 1**).  
**NOTE:** This protocol typically detects six to seven heartbeats in one cine loop. Since the aortic diameter is different between systole and diastole (**Figure 4A-G**), the measurements need to be examined at a consistent phase of the cardiac cycle. Systole is defined from the R wave to the end of the T wave. In general, T waves are difficult to identify in mouse ECG. Therefore, the aortic diameter in systole should be measured at physiologic systole, defined by visual inspection (**Figure 4I**). The cardiac phase when the aorta is maximally expanded should be midsystole. End-diastole is easily defined at the R wave of the ECG (**Figure 4I**). Aortic measurements in end-diastole are simpler than those in midsystole in terms of distinguishing the cardiac cycle.
3. Draw a line in the center of the aortic lumen. This center line will be used to ensure that the measurement lines are perpendicular to the aorta (**Figure 4B,D** and **Supplemental Figure 1**).
4. Draw perpendicular lines through the center line from the luminal inner edge to inner edge at the aortic sinus and maximal ascending aortic levels (**Figure 4B,D** and **Supplemental Figure 1**).
5. Measure the aortic diameter in at least three separate heartbeats and calculate the mean of the measurements.  
**NOTE:** The Vevo2100 system uses the Vevo LAB analysis software for measurements of aortic dimension. Brief explanations for each button are as follows. Measurement mode (**Supplemental Figure 1A**): this mode must be selected for aortic measurements. The slider of a cine loop (**Supplemental Figure 1B**): the ultrasound frame is selected using this slider. Traced distance (**Supplemental Figure 1C**): the center line is drawn with this function. Linear distance (**Supplemental Figure 1D**): the aortic dimension is measured using this function.

### 2. Analysis of abdominal aortic images

1. Launch the analysis software and open the ultrasound data.
2. Select an aortic image for analysis from the cine loop (**Figure 4E,G**).  
**NOTE:** Similar to thoracic aortic measurements, the cardiac cycle may affect the abdominal aortic diameter and area. Measurements should be determined at a consistent phase of the cardiac cycle.
3. Draw a line across the largest luminal diameter, from the inner edge to the inner edge of the vessel lumen (**Figure 4F,H**).
4. Trace the inner edge of the aortic lumen for the luminal area (**Figure 4F,H**).
5. Acquire aortic measurements at a minimum of three separate heartbeats and calculate the mean of the data.

## Representative Results

Representative ultrasound images of nonaneurysmal proximal thoracic and abdominal aorta are shown in **Figure 3A** and **Figure 3C**, respectively. The ascending aorta is located next to the pulmonary artery and forms a curved tube with three branches in the arch region: the innominate artery, the left common carotid artery, and the left subclavian artery (**Figure 3A**). The abdominal aorta is detected dorsally to the inferior vena cava (**Figure 3D**). Representative images of thoracic and abdominal aortic aneurysms with profound dilations, as compared with normal diameters in **Figure 3A** and **Figure 3D**, are shown in **Figure 3B** and **Figure 3H**, respectively. All ultrasound images were captured at end-diastole.

Representative thoracic and abdominal aortic ultrasound images were captured at the midsystole and end-diastole (**Figure 4A,C,E,G**). Representative images showing measurements are presented in **Figure 4B,D,F,H**. The green line in the center of the ascending aorta was used for standardizing the aortic sinus and ascending aortic diameter (**Figure 4B,D**). Lines were drawn perpendicularly to the green line between the two inner edges of the lumen at the aortic sinus (yellow line) and the maximal ascending aortic diameter (red line). The luminal diameters of the thoracic and abdominal aortas were different between systole and diastole (**Figure 4A-H**). For the abdominal aorta, the maximal aortic diameter (red) and luminal area (green) were measured (**Figure 4F,H**). A representative image of the monitor electrocardiogram is shown in **Figure 4I**. The cardiac cycle needs to be considered for accurate measurements. The end-diastole and systole are indicated by the white dotted and pink lines, respectively.

To validate the accuracy and reproducibility of this protocol, we performed a pilot study. Representative thoracic aortic ultrasound and ex vivo images are shown in **Figure 5A**. There was no major difference in diameters measured between these images for the ascending aortic diameter (ultrasound: 1.67 mm vs. ex vivo: 1.65 mm). Since the aortic sinus was difficult to see in the ex vivo image, the aortic sinus diameter was not measured ex vivo. The inter- and intraobserver reproducibility of this protocol are shown in **Figure 5B,C**. To determine potential variabilities, ultrasound imaging was performed by two observers independently, namely by an experienced cardiologist and a nonexperienced undergraduate student who is learning this technique, on two different days, using the same mice ( $n = 5$ ). All dots were located between the mean  $\pm 1.96$  SD in **Figure 5B,C**, which indicates no major inter- or intraobserver variabilities for this protocol.

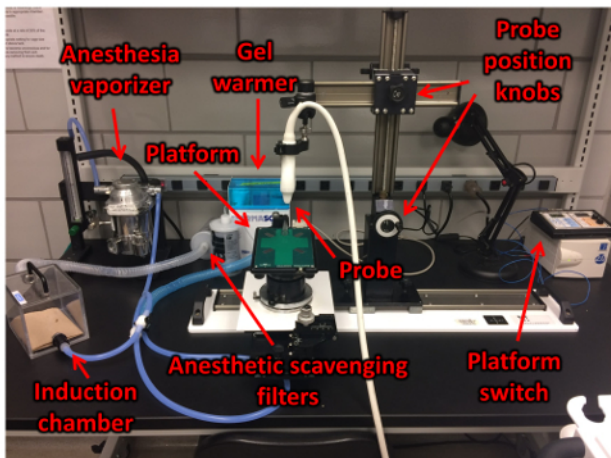


**Figure 1: Workstation setup.** The workstation includes the induction chamber for anesthesia, anesthetic scavenging filters, the heated platform, the ultrasound gel, and the gel warmer. [Please click here to view a larger version of this figure.](#)

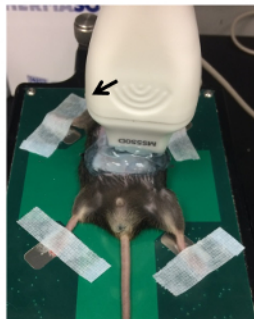
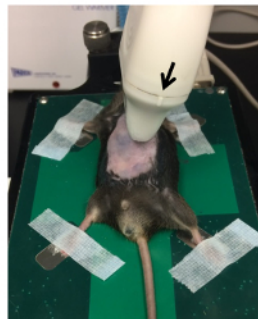
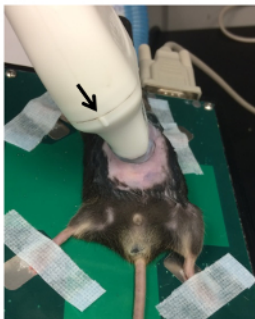
**Thoracic Aorta**

**(A) Right**

**(B) Left**

**Abdominal Aorta**

**(C) Short Axis**



**(D) Ultrasound Image**

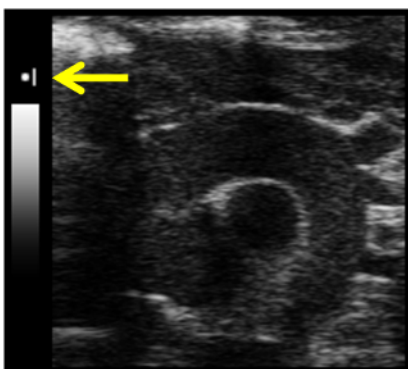


**Figure 2: Examples of probe placement for proximal thoracic and abdominal aortic imaging.** Probe placement for (A) the right and (B) the left parasternal long axis view of the aortic root, ascending and arch regions, and (C) the short axis view of the abdominal aorta. (D) A representative monitor image of the ultrasound system. The black arrows indicate the reference marker on the probe. The yellow arrow indicates the side of the reference marker. [Please click here to view a larger version of this figure.](#)

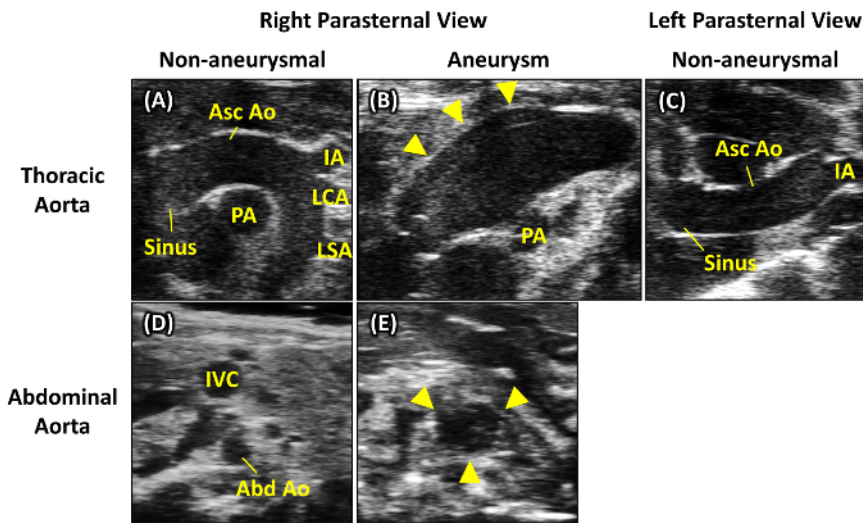


**Figure 3: Representative ultrasound images of the thoracic and abdominal aorta.** (A) Nonaneurysmal and (B) aneurysmal ascending aorta, from the right parasternal long axis view. (C) Nonaneurysmal ascending aorta, from the left parasternal long axis view. (D) Nonaneurysmal and (E) aneurysmal abdominal aorta. Asc Ao = ascending aorta, IA = innominate artery, LCA = left common carotid artery, LSA = left subclavian artery, PA = pulmonary artery, Sinus = aortic sinus, IVC = inferior vena cava, and Abd Ao = abdominal aorta. The yellow triangles indicate an aortic aneurysm. [Please click here to view a larger version of this figure.](#)

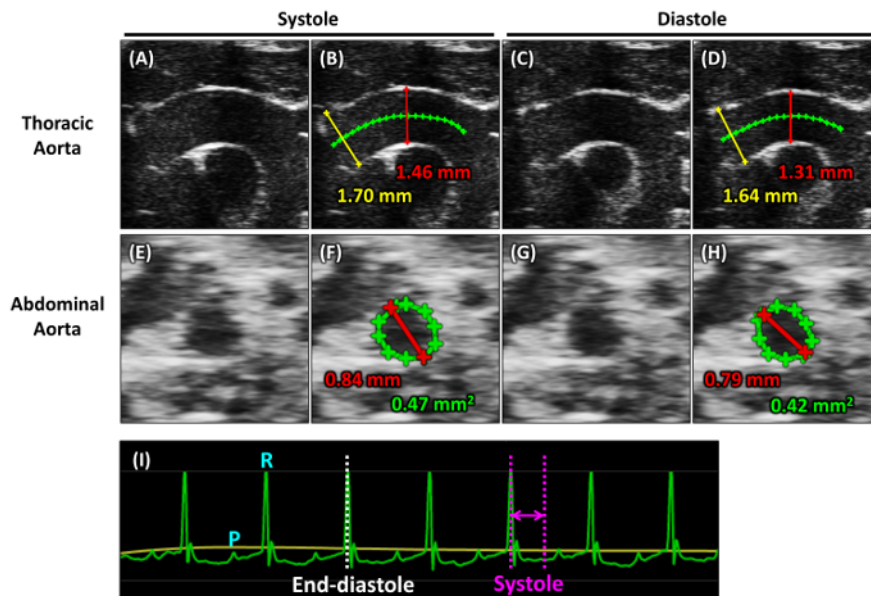


**Figure 4: Measurements of aortic images.** Images of the thoracic aorta captured at (A) the midsystole and (C) the end-diastole. Images showing measurements of aortic diameters in the proximal thoracic aortic region during (B) midsystole and (D) diastole. The green line indicates the center of the ascending aorta. The yellow and red lines indicate diameters of the aortic sinus and ascending aorta, respectively. Digits in yellow and red colors indicate actual diameters of the aortic sinus and ascending aorta, respectively. Images of abdominal aorta captured at (E) the midsystole and (G) the end-diastole. Images showing measurements of the suprarenal aorta during (F) midsystole and (H) end-diastole. The red and green lines indicate the diameter and luminal area of the abdominal aorta, respectively. Digits in red and green colors indicate the actual diameter and area of the abdominal aorta, respectively. (I) Monitor electrocardiogram (ECG) recorded during the image acquisitions. The green and yellow lines indicate the ECG and respiratory cycle, respectively. The white dotted line indicates the end-diastole, and the purple line indicates systole. P = P wave and R = R wave. [Please click here to view a larger version of this figure.](#)

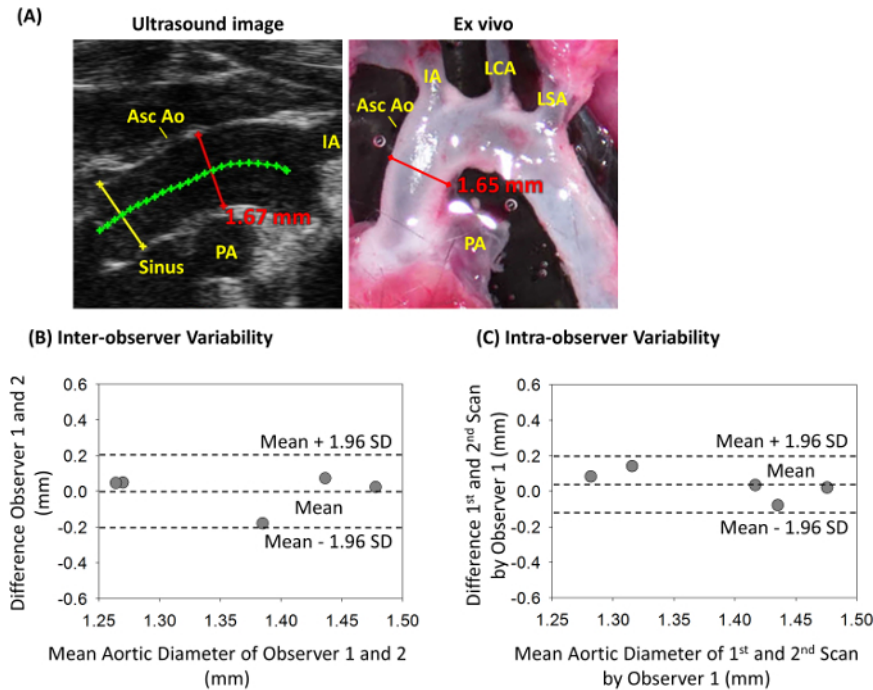
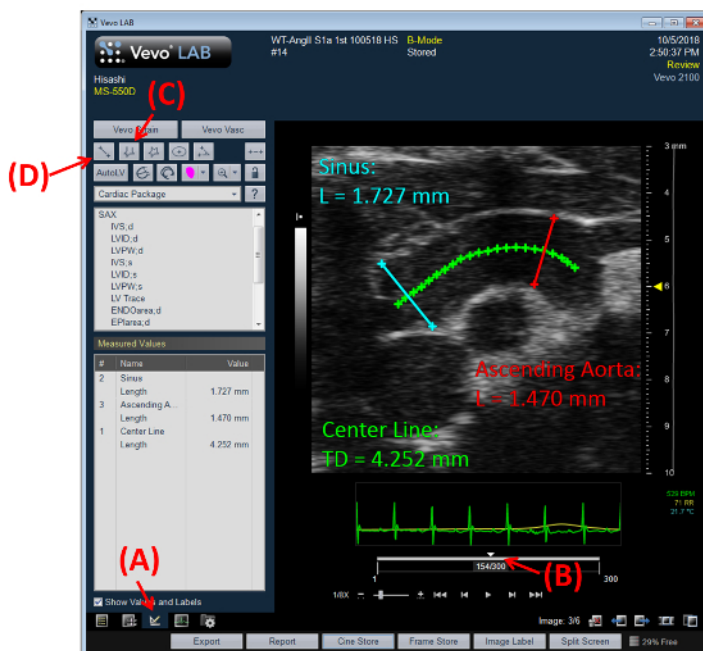


**Figure 5: Accuracy and reproducibility of ultrasound imaging.** (A) Representative images of thoracic aortic ultrasound and ex vivo images in C57BL/6J male mice (10-12 weeks old). Bland-Altman plots show (B) inter- and (C) intraobserver variabilities of this protocol. Asc Ao = ascending aorta, IA = innominate artery, LCA = left common carotid artery, LSA = left subclavian artery, PA = pulmonary artery, and Sinus = aortic sinus. The green line indicates the center of the ascending aorta. The yellow and red lines indicate the diameters of the aortic sinus and ascending aorta, respectively. Digits in red colors denote the actual diameters of the ascending aorta measured in ultrasound and ex vivo images. The black dotted lines indicate the mean and mean  $\pm$  1.96 SD. [Please click here to view a larger version of this figure.](#)



**Supplemental Figure 1: Example image of ultrasound analysis software.** Ultrasound data analysis must be performed in (A) measurement mode. One aortic ultrasound image is selected for analysis from the cine loop using (B) the slider of a cine loop. The center line is drawn using (C) the traced distance function. The aortic dimension is measured by (D) the linear distance function. [Please click here to view a larger version of this figure.](#)

## Discussion

This protocol provides a technical guide for the image acquisition of the thoracic and abdominal aorta in mice, using a high-frequency ultrasound system. Ultrasound aortic imaging has potential confounders, such as probe position and cardiac cycle, that may compromise the accuracy of the aortic measurements, particularly in the proximal thoracic aorta. This protocol describes detailed instructions and strategies for image acquisition, measurement, and data analysis, in order to accurately measure aortic dimensions.

For imaging the proximal thoracic aorta, there are several approaches to probe placement. The right parasternal long axis view shown in **Figure 2A** was used for ultrasound imaging in this protocol. This view facilitates the acquisition of high-quality images from the aortic sinus to the aortic arch portion. It is not optimal for the descending aorta because of interference of the ultrasonic waves. This protocol is applicable to most mouse models of thoracic aortic aneurysms because they exhibit luminal dilation predominantly in the aortic root to the ascending aorta. This includes chronic angiotensin II infusion that causes aneurysm formation in the ascending aorta of mice<sup>18,19,20,21,22,23</sup>. Mouse models of Marfan syndrome (fibrillin 1<sup>C1041G/+</sup> and fibrillin 1<sup>mgR/mgR</sup> mice) display both aortic root and ascending aortic dilation<sup>23,24,25</sup>. Loeys-Dietz syndrome mouse models (postnatal deletion of TGF- $\beta$  receptor 1 or 2 in smooth muscle cells) also develop aneurysm in the aortic root and ascending aorta<sup>18,26,27,28</sup>. Therefore, the right parasternal long axis view is appropriate for aortic imaging in these mouse models of thoracic aortic aneurysms. On the other hand, the right parasternal short axis view has the potential to capture aortic images diagonally because aneurysms are often complicated by aortic tortuosity, which may cause an overestimation of diameters. Unlike the thoracic aorta, the short axis view was used for the imaging of the abdominal aorta in this protocol. Since aortic curvature and tortuosity are modest in the abdominal aorta compared to the thoracic aorta, the acquisition of images in the short axis view ameliorates underestimations of the aortic diameter. It is important to note that different probe positions provide different viewing angles, and the aortic diameter may be different in each view angle. Therefore, reliable aortic diameter measurements are enhanced by applying the same probe position for all images within a study. Interestingly, three-dimensional (3D) ultrasound images of the heart and aorta have been reported recently<sup>29,30,31,32</sup>. In addition, current ultrasound systems can obtain 3D images over time as four-dimensional images<sup>33</sup>. Thus, these 3D imaging technologies have the potential to demonstrate the aortic structure more precisely, which may solve the problem of probe positioning.

Ultrasound images can be captured in either 2D brightness mode (B-mode) or one-dimensional motion mode (M-mode). Although some articles have used M-mode for the measurement of aortic diameter, B-mode is preferable<sup>15,34,35,36</sup>. M-mode has the capacity to image in two dimensions to increase temporal and spatial resolution. However, this mode relies on the assumption that the aorta is a concentric cylinder being imaged perpendicularly to the ultrasonic waves. This assumption may not hold true in an aneurysmal state and the curvature of the ascending aorta makes this difficult, even in nonaneurysmal states. In addition, the aorta does not remain in a fixed position throughout the cardiac cycle<sup>37</sup>. Therefore, M-mode may cause measurement errors, including over- and underestimations.

It is also important to note that the cardiac cycle affects the luminal diameter in the aorta. As expected, the aortic diameter in systole is greater than in diastole (**Figure 4A-H**), which is associated with aortic wall elasticity and strain. Aortic wall elasticity and strain can be calculated from the difference of aortic diameters between systole and diastole. Elasticity and strain are decreased in aneurysmal aortas compared to normal aortas<sup>31,34,35,38,39,40</sup>. Aortic stiffness cannot be measured directly by ultrasound. Measuring pulse wave velocity (PWV) can evaluate its stiffness as a proxy, which is reported to be increased in aneurysmal aortas<sup>31,35,41,42</sup>. PWV is calculated by the transit time between two arterial sites, using pulse wave Doppler images and their corresponding distance. For comparing aortic diameters, unlike clinical examination, there is no rigorous standardization in terms of cardiac phase for aortic measurements in mice. Therefore, it is still unclear which cardiac phase is appropriate for aortic measurements. However, to ensure reliable and reproducible comparisons, aortic diameters should be measured in a defined phase of the cardiac cycle.

This protocol provides detailed instructions for aortic imaging and data analysis in order to measure aortic dimensions accurately. The aortic measurement, using this protocol, was consistent with the actual ex vivo aortic diameter (**Figure 5A**). We also confirmed consistencies of inter- and intraobserver reproducibility (**Figure 5B,C**). All steps in this protocol, especially probe position and cardiac cycle, are necessary for accurate measurements. However, even when using appropriate procedures, artifacts during ultrasound imaging are unavoidable. The location of ribs and lung, as well as respiration and cardiac pulsation, can affect the image quality of the thoracic aorta. Intestinal gas can also cause artifacts in abdominal imaging. Thus, we suggest defining exclusion criteria when following this protocol in case of poor aortic images.

With the advent of high-resolution ultrasound systems, the aortic structure of mice can be examined in exquisite detail, both serially and conventionally, thereby greatly contributing to the understanding of aortic aneurysms. Ultrasound imaging, with the protocol as described above, is a reliable and reproducible noninvasive approach for quantifying aortic aneurysms in mice.

## Disclosures

The authors have nothing to disclose.

## Acknowledgments

The authors' research work was supported by the National Heart, Lung, and Blood Institute of the National Institutes of Health under award numbers R01HL133723 and R01HL139748 and the American Heart Association SFRN in Vascular Disease (18SFRN33960001). H.S. is supported by an AHA postdoctoral fellowship (18POST33990468). J.C. is supported by NCATS UL1TR001998. The content in this manuscript is solely the responsibility of the authors and does not necessarily represent the official views of the National Institutes of Health.

## References

- Hiratzka, L. F., et al. 2010 ACCF/AHA/AATS/ACR/ASA/SCA/SCAI/SIR/STS/SVM guidelines for the diagnosis and management of patients with Thoracic Aortic Disease: a report of the American College of Cardiology Foundation/American Heart Association Task Force on Practice Guidelines, American Association for Thoracic Surgery, American College of Radiology, American Stroke Association, Society of Cardiovascular Anesthesiologists, Society for Cardiovascular Angiography and Interventions, Society of Interventional Radiology, Society of Thoracic Surgeons, and Society for Vascular Medicine. *Circulation*. **121** (13), e266-369 (2010).
- Robinet, P., et al. Consideration of Sex Differences in Design and Reporting of Experimental Arterial Pathology Studies-Statement From ATVB Council. *Arteriosclerosis, Thrombosis, and Vascular Biology*. **38** (2), 292-303 (2018).
- Wanhainen, A., Mani, K., Golledge, J. Surrogate Markers of Abdominal Aortic Aneurysm Progression. *Arteriosclerosis, Thrombosis, and Vascular Biology*. **36** (2), 236-244 (2016).
- Lu, H., Daugherty, A. Aortic Aneurysms. *Arteriosclerosis, Thrombosis, and Vascular Biology*. **37** (6), e59-e65 (2017).
- Angelov, S. N., Zhu, J., Dichek, D. A. New Mouse Model of Abdominal Aortic Aneurysm: Put Out to Expand. *Arteriosclerosis, Thrombosis, and Vascular Biology*. **37** (11), 1990-1993 (2017).
- Daugherty, A., Manning, M. W., Cassis, L. A. Angiotensin II promotes atherosclerotic lesions and aneurysms in apolipoprotein E-deficient mice. *The Journal of Clinical Investigation*. **105** (11), 1605-1612 (2000).
- Kanematsu, Y., et al. Pharmacologically induced thoracic and abdominal aortic aneurysms in mice. *Hypertension*. **55** (5), 1267-1274 (2010).
- Longo, G. M., et al. Matrix metalloproteinases 2 and 9 work in concert to produce aortic aneurysms. *The Journal of Clinical Investigation*. **110** (5), 625-632 (2002).
- Pyo, R., et al. Targeted gene disruption of matrix metalloproteinase-9 (gelatinase B) suppresses development of experimental abdominal aortic aneurysms. *The Journal of Clinical Investigation*. **105** (11), 1641-1649 (2000).
- Raffort, J., et al. Monocytes and macrophages in abdominal aortic aneurysm. *Nature Reviews Cardiology*. **14** (8), 457-471 (2017).
- Senemaud, J., et al. Translational Relevance and Recent Advances of Animal Models of Abdominal Aortic Aneurysm. *Arteriosclerosis, Thrombosis, and Vascular Biology*. **37** (3), 401-410 (2017).
- Wilson, N. K., Gould, R. A., Gallo MacFarlane, E., Consortium, M. L. Pathophysiology of aortic aneurysm: insights from human genetics and mouse models. *Pharmacogenomics*. **17** (18), 2071-2080 (2016).
- Adam, M., et al. Systemic Upregulation of IL-10 (Interleukin-10) Using a Nonimmunogenic Vector Reduces Growth and Rate of Dissecting Abdominal Aortic Aneurysm. *Arteriosclerosis, Thrombosis, and Vascular Biology*. **38** (8), 1796-1805 (2018).
- Barisione, C., et al. Rapid dilation of the abdominal aorta during infusion of angiotensin II detected by noninvasive high-frequency ultrasonography. *Journal of Vascular Surgery*. **44** (2), 372-376 (2006).
- Trachet, B., et al. Ascending Aortic Aneurysm in Angiotensin II-Infused Mice: Formation, Progression, and the Role of Focal Dissections. *Arteriosclerosis, Thrombosis, and Vascular Biology*. **36** (4), 673-681 (2016).
- Sawada, H., et al. Heterogeneity of aortic smooth muscle cells: A determinant for regional characteristics of thoracic aortic aneurysms? *Journal of Translational Internal Medicine*. **6** (3), 93-96 (2018).
- Davis, F. M., et al. Smooth muscle cell deletion of low-density lipoprotein receptor-related protein 1 augments angiotensin II-induced superior mesenteric arterial and ascending aortic aneurysms. *Arteriosclerosis, Thrombosis, and Vascular Biology*. **35** (1), 155-162 (2015).
- Angelov, S. N., et al. TGF-beta (Transforming Growth Factor-beta) Signaling Protects the Thoracic and Abdominal Aorta From Angiotensin II-Induced Pathology by Distinct Mechanisms. *Arteriosclerosis, Thrombosis, and Vascular Biology*. **37** (11), 2102-2113 (2017).
- Daugherty, A., et al. Angiotensin II infusion promotes ascending aortic aneurysms: attenuation by CCR2 deficiency in apoE-/- mice. *Clinical Science*. **118** (11), 681-689 (2010).
- Fava, M., et al. Role of ADAMTS-5 in Aortic Dilatation and Extracellular Matrix Remodeling. *Arteriosclerosis, Thrombosis, and Vascular Biology*. **38** (7), 1537-1548 (2018).
- Rateri, D. L., et al. Angiotensin II induces region-specific medial disruption during evolution of ascending aortic aneurysms. *The American Journal of Pathology*. **184** (9), 2586-2595 (2014).
- Huang, X., et al. MicroRNA-21 Knockout Exacerbates Angiotensin II-Induced Thoracic Aortic Aneurysm and Dissection in Mice With Abnormal Transforming Growth Factor-beta-SMAD3 Signaling. *Arteriosclerosis, Thrombosis, and Vascular Biology*. **38** (5), 1086-1101 (2018).
- Galatioto, J., et al. Cell Type-Specific Contributions of the Angiotensin II Type 1a Receptor to Aorta Homeostasis and Aneurysmal Disease- Brief Report. *Arteriosclerosis, Thrombosis, and Vascular Biology*. **38** (3), 588-591 (2018).
- Habashi, J. P., et al. Losartan, an AT1 antagonist, prevents aortic aneurysm in a mouse model of Marfan syndrome. *Science*. **312** (5770), 117-121 (2006).
- Hibender, S., et al. Resveratrol Inhibits Aortic Root Dilatation in the Fbn1C1039G/+ Marfan Mouse Model. *Arteriosclerosis, Thrombosis, and Vascular Biology*. **36** (8), 1618-1626 (2016).
- Hu, J. H., et al. Postnatal Deletion of the Type II Transforming Growth Factor-beta Receptor in Smooth Muscle Cells Causes Severe Aortopathy in Mice. *Arteriosclerosis, Thrombosis, and Vascular Biology*. **35** (12), 2647-2656 (2015).
- Li, W., et al. Tgfr2 disruption in postnatal smooth muscle impairs aortic wall homeostasis. *The Journal of Clinical Investigation*. **124** (2), 755-767 (2014).
- Yang, P., et al. Smooth muscle cell-specific Tgfr1 deficiency promotes aortic aneurysm formation by stimulating multiple signaling events. *Scientific Reports*. **6**, 35444 (2016).
- Dawson, D., et al. Quantitative 3-dimensional echocardiography for accurate and rapid cardiac phenotype characterization in mice. *Circulation*. **110** (12), 1632-1637 (2004).
- Grune, J., et al. Evaluation of a commercial multi-dimensional echocardiography technique for ventricular volumetry in small animals. *Cardiovascular Ultrasound*. **16** (1), 10 (2018).
- Phillips, E. H., Di Achille, P., Bersi, M. R., Humphrey, J. D., Goergen, C. J. Multi-Modality Imaging Enables Detailed Hemodynamic Simulations in Dissecting Aneurysms in Mice. *IEEE Transactions on Medical Imaging*. **36** (6), 1297-1305 (2017).
- Soepriatna, A. H., Damen, F. W., Vlachos, P. P., Goergen, C. J. Cardiac and respiratory-gated volumetric murine ultrasound. *The International Journal of Cardiovascular Imaging*. **34** (5), 713-724 (2018).
- FUJIFILM VisualSonics Inc. *Vevo3100 - the ultimate preclinical imaging experience*. (2018).



34. Shen, M., et al. Divergent roles of matrix metalloproteinase 2 in pathogenesis of thoracic aortic aneurysm. *Arteriosclerosis, Thrombosis, and Vascular Biology*. **35** (4), 888-898 (2015).
35. Trachet, B., et al. Performance comparison of ultrasound-based methods to assess aortic diameter and stiffness in normal and aneurysmal mice. *PLoS One*. **10** (5), e0129007 (2015).
36. Wang, Y., et al. TGF-beta activity protects against inflammatory aortic aneurysm progression and complications in angiotensin II-infused mice. *The Journal of Clinical Investigation*. **120** (2), 422-432 (2010).
37. Goergen, C. J., et al. In vivo quantification of murine aortic cyclic strain, motion, and curvature: implications for abdominal aortic aneurysm growth. *Journal of Magnetic Resonance Imaging*. **32** (4), 847-858 (2010).
38. Ben-Zvi, D., et al. Local Application of Leptin Antagonist Attenuates Angiotensin II-Induced Ascending Aortic Aneurysm and Cardiac Remodeling. *Journal of the American Heart Association*. **5** (5) (2016).
39. Goergen, C. J., et al. Influences of aortic motion and curvature on vessel expansion in murine experimental aneurysms. *Arteriosclerosis, Thrombosis, and Vascular Biology*. **31** (2), 270-279 (2011).
40. Phillips, E. H., et al. Morphological and Biomechanical Differences in the Elastase and AngII apoE(-/-) Rodent Models of Abdominal Aortic Aneurysms. *BioMed Research International*. **2015**, 413189 (2015).
41. Di Lascio, N., Kusmic, C., Stea, F., Faita, F. Ultrasound-based Pulse Wave Velocity Evaluation in Mice. *Journal of Visualized Experiments*. (120), e54362 (2017).
42. Lee, L., et al. Aortic and Cardiac Structure and Function Using High-Resolution Echocardiography and Optical Coherence Tomography in a Mouse Model of Marfan Syndrome. *PLoS One*. **11** (11), e0164778 (2016).